

PHOENIX-2: A New Broadband Spectrometer for Decimetric and Microwave Radio Bursts

First Results

Peter Messmer, Arnold O. Benz and Christian Monstein

Institute of Astronomy, ETH, CH-8092 Zürich, Switzerland

Abstract. A broadband radio spectrometer has been put into operation at Bleien, Switzerland, to register the flare emission of the full sun. In the frequency range of operation, 0.1 to 4.0 GHz, both modes of circular polarization are recorded continuously. The new system, *Phoenix-2*, has been developed from the experience with the previous *Phoenix* spectrometer. Improved, computer controlled focal hardware allows now a complete daily calibration, a more sophisticated calibration procedure, and monitoring of all essential instrumental and environmental parameters. Calibrated data is now usually available the day after observation and is accessible through the Internet. The scientific improvements include a larger frequency range of observation, a larger number of completely recorded events due to full-day registration, more accurate measurements, particularly in circular polarization, and more reliable operation. First observations are presented and quantitative results comparing the calibration with single frequency instruments are reported.

Keywords: Instruments

1. Introduction

Non-thermal particles accelerated in solar flares are well known to generate various kinds of waves in the coronal plasma. Flare energy release, requiring possibly anomalous resistivity, may be itself a source of such waves. Many of these waves in the plasma are capable to be transformed into propagating electromagnetic waves, and some of the latter may be observable as coherent radio bursts. The energy of major flares is released in the lower corona of active regions. Particle acceleration is generally modeled in a plasma having an electron density between 10^9 and 10^{11} cm^{-3} and a magnetic field of 100 to 1000 Gauss (e.g. Miller et al., 1997). If the energy release process or the particle excite plasma waves in or near the acceleration region, the observable radio emission should be roughly in the range between 0.3 and 6 GHz. For maser emission at the fundamental of the electron gyrofrequency, the emission would be the range from 0.3 and 3 GHz, and for harmonics at an accordingly higher frequency. Although the excitation of these waves may be very likely, they have to overcome enormous absorption of the ambient plasma to escape the corona.



It is known since the early 1960s (Young et al., 1961), that some flares emit intense coherent decimetric radiation. The emission is easily distinguished from the incoherent, very broadband gyrosynchrotron emission. A combination of density inhomogeneity, emitting region being located in high-density regions, scattering and ducting makes it possible that coherent emission at the mentioned characteristic plasma frequencies can escape. It carries information on the flare energy release process and/or its accelerated particles.

The Radio Astronomy and Plasma Physics (RAPP) group of the Institute of Astronomy at the Swiss Federal Institute of Technology (ETH) in Zurich has been engaged in spectral investigations of solar radio bursts since 1972.

The analog-recording spectrograph *Daedalus* registered events in the 0.1 – 1.0 GHz range for more than one solar cycle. Its computer-controlled successor, *Ikarus*, provided higher temporal and spectral resolution beside digital recording capabilities (Perrenoud, 1982). A survey of decimetric emissions in the 0.1 – 1.0 GHz range (Güdel and Benz, 1990) and many investigations on narrow-band spikes are among the major observations performed with *Icarus* (e.g. Benz, 1985; Aschwanden and Güdel, 1992; Benz, Csillaghy, and Aschwanden, 1996). The spectrometer *Phoenix* extended the frequency range to 3 GHz and temporarily up to 8.5 GHz (Benz et al., 1991). This allowed to extend the catalog of decimetric emissions (Bruggmann et al., 1990; Isliker and Benz, 1994), to resolve microwave narrow-band spikes in frequency and to determine their decay times at higher frequencies (Güdel and Benz, 1990; Csillaghy and Benz, 1993).

After several years of operation, the *Phoenix* system has now been redesigned. While parts of the receiver hardware were reused in the emerging system, all of the dedicated control hardware was replaced by PC controlled components. The system is designed for complete autonomous operation, including data transfer to the Institute of Astronomy in Zurich, data calibration and data archiving.

This paper is organized in the following way: The next section gives an overview of the *Phoenix-2* hardware and a list of system parameters. Sec. 3 describes the new organization of data transfer and processing, and Sec. 4 the calibration procedure with calibration results in Sec. 5. Sec. 6 shows some first observational results, obtained with the new system. Conclusions are given in Sec. 7.

2. Hardware

The frequency-agile radio spectrometer *Phoenix-2* of ETH is located at Bleien, about 50 km west of Zürich, Switzerland. The system is fed by a parabolic dish of 7 m diameter, which is pointed continuously to the sun. The position is controlled by two 11-bit angular decoders.

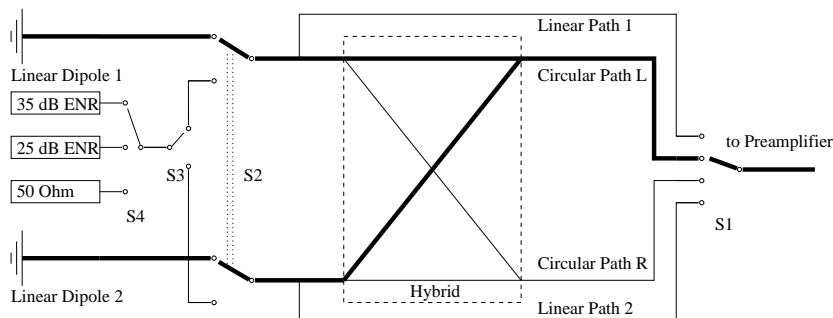


Figure 1. Simplified scheme of the front-end high-frequency paths. All open switches are terminated with a 50 Ohm resistor. Switch S_1 selects between linear polarization and circular polarization measurement. Switch S_2 connects either both sets of dipoles or a noise source to the high-frequency paths. In the latter case, switch S_3 selects the path to which the noise source is connected, and switch S_4 finally selects one of three different noise sources. The highlighted path shows, as an example, the configuration for left circular polarization measurements.

In the primary focus, two sets of crossed log-periodic dipoles, covering a range from 0.1-4 GHz, and a thermally stabilized front end are installed.

A simplified scheme of the front end circuits is shown in Fig. 1. The radiation is captured by the two orthogonal sets of dipoles on the left hand side of the picture and guided through one of four high-frequency channels to the pre-amplifier on the right hand side. Switch S_1 selects either linear or circular polarization measurements. In case of linear measurement, one set of linear dipoles is connected directly to the pre-amplifier (linear paths 1 and 2). In case of circular polarization measurements, both sets of dipoles are connected to a hybrid, introducing a phase shift of $\pm\pi/2$ between the two linear paths. One of the hybrid output terminals is then connected to the pre-amplifier (circular paths L and R). Switch S_2 connects either the dipoles or a noise source to the high-frequency paths. In the latter case, switch S_3 determines to which high-frequency path the noise source is connected to and switch S_4 finally selects between the noise sources at either 35 dB ENR, 25 dB ENR or terminated with 50 Ohm.

Switch S_1 is realized by cascading PIN-Diode switches and mechanical relays, allowing to switch between two states of polarization

(circular L - circular R or linear 1 - linear 2) in less than 15 ns. The same design was chosen for switch S_2 , allowing Dicke measurements by switching between dipoles and a noise source.

Table I. *Phoenix-2* system specification.

Parameter	Phoenix-2
Frequency range	0.1 – 4 GHz
Number of channels (maximum)	2000
Channel bandwidth	1, 3 or 10 MHz
Integration time per channel	440 μ s
Temporal resolution	500 μ s with 1 channel - 1 s with 2000 channels
Recording time	sunrise - sunset
Antenna	7 m parabola
Focal ratio	0.34
Effective antenna area	15 m ² @ 0.6 GHz - 0.5 m ² @ 4 GHz
System temperature	1200K @ 0.6 GHz - 2100 K @ 4GHz
Total system gain	16.5 dB

One measurement cycle of 500 μ s duration consists of four individual integration periods of 110 μ s. Between each of them switches S_1 and S_2 can change position. This leads to a total integration time of 220 μ s for combined total flux density and polarization measurements and 440 μ s for single polarization state measurements.

Spectra are obtained by stepping through a set of predefined frequency channels. The number of channels has to be compromised between temporal resolution (500 μ s for single channel measurements) and spectral resolution (2000 channels with one measurement per second in every channel).

The signal for frequency up-conversion to the intermediate frequencies between 8.17 and 11.17 GHz is generated by two alternating synthesizers. While one synthesizer is involved in a given measurement, the other one stabilizes for the next frequency, allowing a high switching rate between stable frequencies. After down-conversion to a second intermediate frequency at 70 MHz and bandwidth selection (1, 3 or 10 MHz) the signal is logarithmically detected in a dynamical range of 80 dB.

Two integrators sum the detector signal during one measurement cycle, one with constant sign, the other one with alternating sign every

second integration period. Switching between left and right polarization, this measures both Stokes I (left plus right circular polarization) and Stokes V (left minus right polarization). After one measurement cycle, these two values are A/D converted and fetched by a PC.

3. Data Transfer and Processing

At the observatory site, two standard PC perform all data acquisition and hardware control. Selection of observed frequencies and initiation of calibration measurements is performed fully autonomous according to predefined schedules.

Every night, the daily data is transferred through the Internet from the observatory location to the Institute of Astronomy in Zurich. The amount of 100-200 MB raw data per day is received through the 128 kbit/s link in 2-4 hours, depending on the network load.

At the receiving site, the incoming data stream is searched for calibration data. If a full set of calibration measurements is available, the system parameters are re-determined. Observational data is calibrated according to the latest determined system parameters. For quicker localization of radio events, the data is compressed into overview spectrograms with reduced temporal and spectral resolution.

Beside the actual observations, additional data is acquired for system control: local weather conditions, noise source temperature, humidity etc. This data is mainly used for quality control and system specification.

The complete data archive is publicly accessible under <http://www.astro.phys.ethz.ch/rag/>. In normal operation, the observational data is available on the following day.

4. Calibration

Calibration of *Phoenix-2* is performed in two steps: In a first step, the receiver calibration, the correspondence between system output and antenna temperature is established. In a second step, the effective antenna area is determined, what allows to transform antenna temperatures into solar flux units. All system parameters are assumed to be frequency dependent, so all calibration steps described in the following are performed for every frequency channel.

4.1. LINEAR POLARIZATION MEASUREMENTS

The receiver system with the logarithmic detector in case of linear polarization measurement is modeled by

$$\rho = A + B \log[\eta_i(T - T_0) + T_s] \quad (1)$$

where ρ is the detector output, A is the system offset, B is the system gain, η_i is the attenuation between noise source and detector, measured through high-frequency path $i \in \{1, 2\}$, T is the antenna temperature, T_0 the constant temperature of the front-end, and T_s the system temperature.

Measuring the three noise sources through both linear paths leads to an overall set of six measurement values for the five unknown system parameters A , B , η_i and T_s . This over-determined system is solved by means of a numerical non-linear optimization.

Knowing the system parameters, the system output can be converted into antenna temperature. To convert now the antenna temperature into solar flux values, the effective antenna area has to be determined,

$$S = \frac{2}{A_e} k_B (T - T_B) \quad (2)$$

where S is the solar flux density, A_e the effective antenna area, k_B the Boltzmann constant, T the antenna temperature and T_B the temperature of the background. Knowing T_B from measurements of the sky off the sun (e.g. during the night), and knowing the solar flux density published by other groups (e.g. NOAA, [gopher://solar.sec.noaa.gov:70/00/lists/radio/rad](http://solar.sec.noaa.gov:70/00/lists/radio/rad)), the effective antenna area can be computed.

4.2. CIRCULAR POLARIZATION MEASUREMENTS

The calibration process for circular polarization measurements is more involved, due to the higher complexity of the high-frequency paths. A major problem is the mixing of both states of circular polarization in the hybrid. The temperature \tilde{T}_L at the hybrid output terminal for left polarization is given by

$$\tilde{T}_L = \frac{1}{2} [T_L(\sigma_{1L} + \sigma_{2L})^2 + T_R(\sigma_{1L} - \sigma_{2L})^2] \quad (3)$$

where T_L, T_R are the antenna temperatures for hypothetical circular polarized antennas, and σ_{ij}^{-2} are the high-frequency path attenuations between noise source and detector, measured through the hybrid between input terminal $i \in \{1, 2\}$ and output terminal $j \in \{L, R\}$.

In case of an ideal hybrid with identical attenuations $\sigma_{1j} = \sigma_{2j}$, there is no mixing between the two antenna temperatures. However, measurements at a network analyzer showed unequal attenuations, making a more elaborated calibration routine necessary.

Measuring the three noise sources through all four hybrid paths leads to a set of 12 measurement values. The overall set of unknown system parameters for circular polarization measurements consists of the four attenuations σ_{ij} in the hybrid, the system temperature T_s , the system gain B , and system offset A , what is a set of seven unknown parameters. This allows to determine all parameters by means of a numerical fit.

5. Calibration Results

Calibration measurements are performed once during night (off sun) and once during daytime (on sun). Beside computation of the receiver parameters, these measurements allow to determine the effective antenna are, according to Sec. 4.1. As solar flux density reference values, the data of the USAF Observatory in Learmonth, Australia (see NOAA, [gopher://solar.sec.noaa.gov:70/00/lists/radio/rad](http://solar.sec.noaa.gov:70/00/lists/radio/rad)) at frequencies 245 MHz, 410 MHz, 610 MHz, 1415 MHz, 2695 MHz, 2800 MHz and 4995 MHz is incorporated into the current calibration.

A way to estimate the accuracy of the model parameters is to compare the parameters determined during an on-sun calibration with those determined off sun. Excluding long time variations, the parameters should be identical in both cases. As the measurements scatter, the numerical uncertainties lead to variations in the parameters. To estimate the resulting error, the variation of the value determined on-sun and off-sun was measured for every system parameter for 16 calibrations. The relative error in the flux density induced by this variation is plotted in the Fig. 2. Based on these errors, the overall error in flux density is estimated.

In the range from 300 MHz to 4 GHz, the total solar flux density is rarely below 40 sfu. In this flux range, the total error is below 10%, promising well calibrated flux density measurements.

Fig. 3 shows peak flux density values for 10 bursts at 1415 MHz, between August and November 1998. The error bars indicate the total system parameter error as shown in Fig. 2. The pre-burst background was subtracted. Quantitatively good agreement was found throughout the range of available flux density values.

Another indicator for the accuracy of the determined flux density is the comparison of the rms flux density noise ΔF with the theoretically

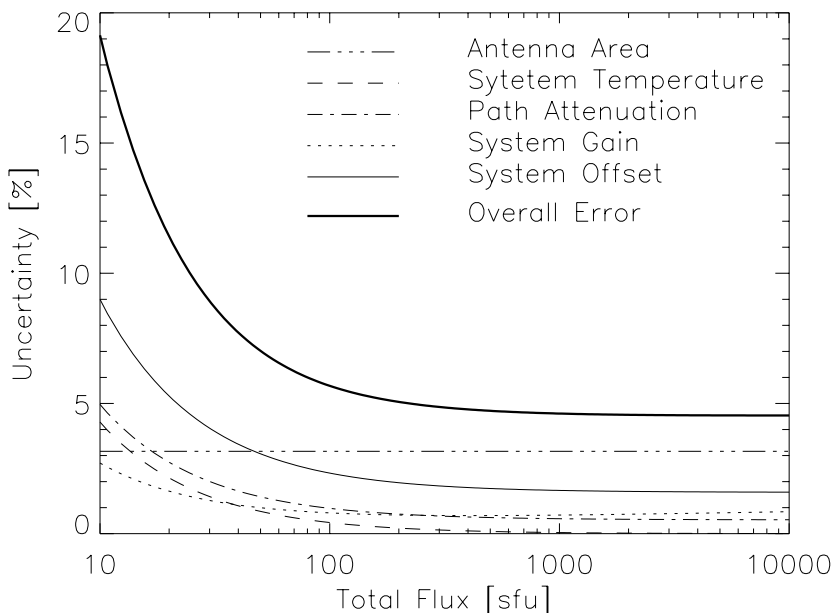


Figure 2. Different sources of uncertainty in absolute flux density measurements, based on model parameter variations in 16 calibrations, as function of determined flux density (at 1415 MHz): system offset A (solid, thin), system gain B (dotted), system temperature T_s (dashed), high-frequency path attenuation η_i (dash-dotted), antenna area (dash-triple-dotted) and theoretical overall error (solid, thick). Up to about 50 sfu total flux, the error is dominated by the uncertainty in the system offset, whereas for higher fluxes the error is dominated by the uncertainty in the effective antenna area. In the range of observation above 40 sfu (which is about the quiet sun background at 300 MHz), the overall error is well below 10 %.

expected rms noise ΔF_T determined by the radiometer equation

$$\Delta F_T = \frac{F}{\sqrt{\Delta\nu\Delta t}} \quad (4)$$

where F is the observed mean flux density, $\Delta\nu$ is the receiver bandwidth and Δt is the total integration period.

At a frequency of 1415 MHz, the measured flux density noise for 440 measurements was

$$\Delta F = (1.01 \pm 0.10)\Delta F_T \quad (5)$$

at a mean flux density of 103 sfu. The given accuracy is the standard deviation, i.e. the half-width of the distribution of single measurements with 10 MHz receiver bandwidth and a total integration time of $220\mu\text{s}$.

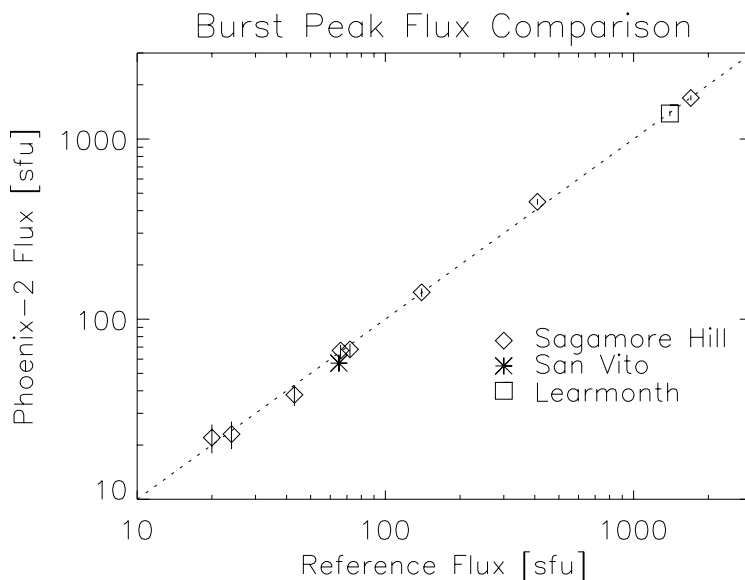


Figure 3. Peak flux density values at 1415 MHz for selected bursts measured by the USAF Stations Sagamore Hill (\diamond), San Vito (*), Learmonth (\square), compared to the values determined by Phoenix-2. The values correspond well over the observed range from 23 sfu - 1400 sfu. (Background flux density between 80 and 110 sfu)

The polarization calibration was investigated by measuring spectra of the communication satellites Intelsat-803 and Arabsat-2B for which the polarization is known. Highly active circular polarized frequency channels were measured as up to 97% polarized. Assuming perfectly circular polarized emitting antennas, this leaves a crosstalk of about 1.5% between left and right circular polarization.

6. First Results

Fig. 4 shows total flux density and polarization measurements of an event on September 23, 06:53:60 - 06:56:00 UT in 33 equidistant-distant frequency channels between 1000 MHz and 2280 MHz. Both abscissa scales are logarithmically compressed. The lower picture shows polarization values for right circular polarization with the pre-flare polarization subtracted. At low total flux density, the polarization measurement exhibits more noise. However, some structures above the smooth continuum are more clearly visible in polarization than in total flux density measurements.

Another example, recorded on September 11, 1998 in the 0.1 to 4 GHz range, is shown in Fig. 5. Due to the high-frequency coverage, the

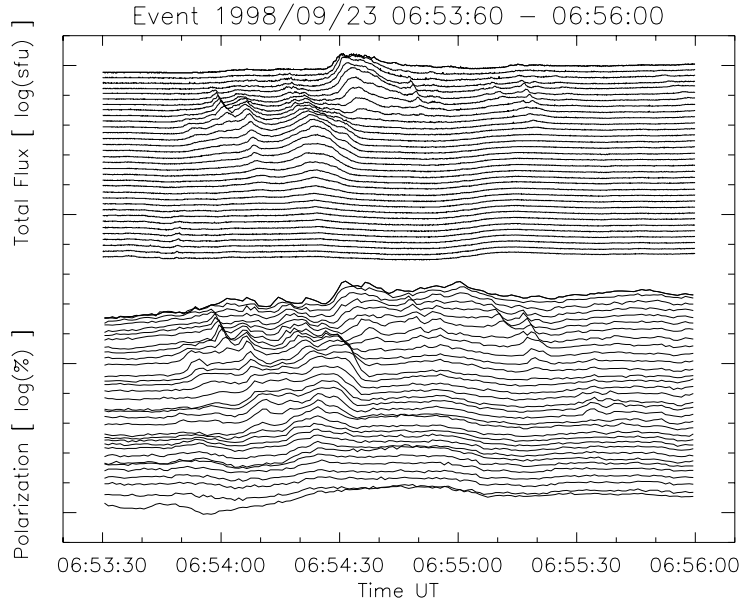


Figure 4. Total flux density (top) and polarization measurements (bottom) of the event 1998/09/23, 06:53:60 - 06:56:00 in 33 equidistant-distant frequency channels between 1000 MHz (top end) and 2280 MHz (lower end). Flux density values are integrated over 0.1 s, leading to an overall integration time of 1.25 ms per bin, whereas polarization values are integrated over 1 s, leading to an overall integration time of 12.5 ms per bin. Both flux and polarization are compressed logarithmically. Several structures show up in polarization, which disappear in the total flux density measurement. An acoustic representation of this event is presented on the enclosed CD-ROM.

temporal resolution was relatively low (0.1 s between measurements in the same frequency channel). The main Type II like structure occurred between 16:02 and 16:09 UT and is depicted in the background picture. The top inset shows a sequence of inverted U-bursts, occurring in the impulsive phase. A background has been subtracted.

The middle inset is a zoom of the impulsive phase in the 1 - 3 GHz range. It shows small-scale structures at frequencies well above those of the type U-bursts. A zoom on these small scale structures (bottom inset) allows to identify them again as type U-bursts, with a turnover frequency of about 1750 MHz.

This event shows clearly the benefit of continuous recording: Small scale events in the impulsive phase can be searched, independent of a burst detection system.

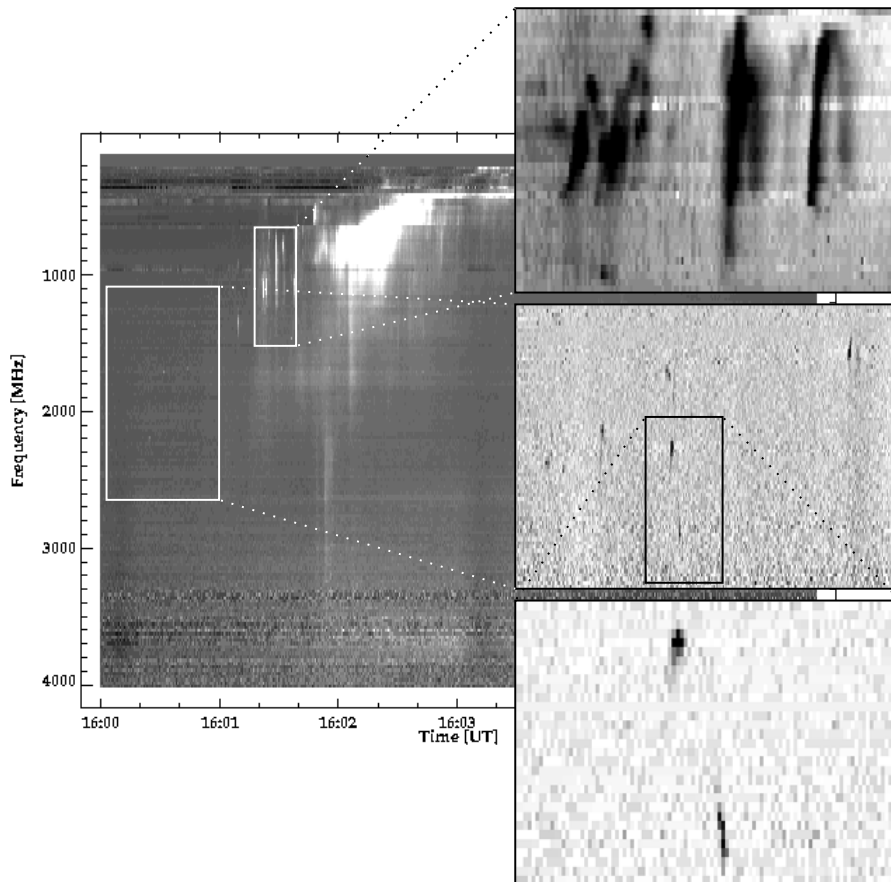


Figure 5. Event of 1998/09/11, 16:00-16:06 in the range of 100 MHz to 4000 MHz. The background picture gives an overview of the total event. Breaks in the spectra are due to missing data. The top inset shows a sequence of U-bursts in the impulsive phase. The middle inset displays a detail of the impulsive phase in the range of 1000 MHz to 3000 MHz, exhibiting small scale emissions. The bottom inset is a detail of the middle inset, showing a turning point in one of these small scale bursts at about 1750 MHz. An acoustic representation of parts of this event is presented on the enclosed CD-ROM.

7. Conclusions

The new radio spectrometer *Phoenix-2* with enhanced capabilities became operational. Similar to the previous instrument, the free choice of the number, bandwidth and frequency of the observed channels makes *Phoenix-2* very flexible for both broadband surveys as well as specific studies at high temporal or spectral resolution. Thus it can be used for both joint observations with instruments observing in other wavelengths and for independent, specific measurements.

Compared to its predecessors, it offers a larger total bandwidth of observation, and full day-time data recording. The data transfer to the processing and archiving computer occurs daily and is fully automatic. A new calibration procedure has been developed, based on new instrumentation in the antenna focus. The observations are calibrated and available in public with one day delay. Burst lists, daily overview spectrograms and other information are available on the Web (<http://www.astro.phys.ethz.ch/rag/>). It is planned to improve and to operate the instrument throughout the new solar cycle.

Acknowledgements

This paper is dedicated to the memory of the late Christoph Zmoos, whose assertive and dedicated work was essential in completing the *Phoenix-2* instrument and whose companionship we are missing.

The original design of the *Phoenix-2* hardware was made by W. Stehling. Much of the new hardware has been developed by Th. Habermacher and C. Zmoos. Important software has been contributed by A. Csillaghy. Thanks are due to F. Aebersold for his mechanical work. The construction of the Zurich radio spectrometers is financed by the Swiss National Science foundation, Grant No. 20-53664.98. The daily solar flux values are contributed by the U.S. Department of Commerce, NOAA, Space Environment Center.

Appendix

Measurements from broadband radio spectrometers are commonly displayed in dynamic spectrograms, showing measured flux density as a function of time and frequency. On the CD enclosed, measurements performed with the new instrument are represented in an acoustic way. Acoustic samples for type III bursts, type U bursts, and narrowband decimetric spikes are presented.

References

- Aschwanden M.J., and Güdel M., 1992, *ApJ* **401**, 736
Benz A.O., 1985, *Solar Phys.* **96**, 357
Benz, A.O., Güdel, M., Isliker, H., Miskowicz, S., and Stehling, W. 1991, *Solar Phys.*, **133**, 385
Benz A.O., Csillaghy A., and Aschwanden M.J., 1996, *A&A* **309**, 291

- Bruggmann, G., Benz, A.O., Magun, A., and Stehling, W.: 1990, *Astron. Astrophys.* **240**, 506.
- Csillaghy A., and Benz A.O., 1993, *A&A*, **274**, 487
- Güdel M., and Benz A.O., 1990, *A&A* **231**, 202
- Islaker H., and Benz A.O., 1994, *A&AS* **104**, 145
- Miller, J.A., Cargill, P.J., Emslie, A.G., Holman, G.D, Dennis, B.R., LaRosa T.N., Winglee, R.M, Benka, G.S., and Tsuneta, S., 1997, *Journal of Geophys. Res.* **102**, 14631
- Perrenoud, M.R.: 1982, *Solar Phys.* **81**, 197.
- Young, C.W., Spencer, C.L., Moreton, G.E., and Roberts, J.A.:1961, *Astrophys.J.* **133**, 243.
- Radio Astronomy and Plasma Physics Group, ETH Zürich, <http://www.astro.phys.ethz.ch/rag/>
- U.S. Department of Commerce, NOAA, Space Environment Center, gopher://solar.sec.noaa.gov:70/00/lists/radio/rad

